IMPLICATION OF STRESS RANGE FOR INELASTIC ANALYSIS

M. E. Karabin

A. K. Dhalla

Westinghouse Electric Corporation
Advanced Reactors Division
Madison, PA

Prepared for the U.S. Department of Energy
Division of Reactor Reasearch and Development
Under Contract Number DE-AC15-76CL02395

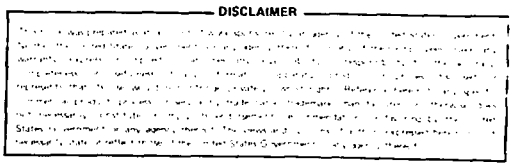

Westinghouse Electric Corporation
Advanced Reactors Division
P. O. Box 158
Madison, Pennsylvania 15663

ABSTRACT

The elastic stress range over a complete load cycle is routinely used to formulate simplified rules regarding the inelastic behavior of structures operating at elevated temperature. For example, a 300 series stainless steel structure operating at elevated temperature, in all probability, would satisfy the ASME Boiler and Pressure Vessel Code criteria if the linearized elastic stress range is less than three times the material yield strength. However, at higher elastic stress ranges it is difficult to judge, a priori, that a structural component would comply with inelastic Code criteria after a detailed inelastic analysis. The purpose of this paper is to illustrate that it is not the elastic stress range but the stress intensities at specific times during a thermal transient which provide a better insight into the inelastic response of the structure. The specific example of a flued head design demonstrates that the temperature differential between various parts of the structure can be changed by modifying the insulation pattern and heat flow path in the structure, without significantly altering the elastic stress range over a complete load cycle. However, the modified design did reduce the stress intensity during steady state elevated temperature operation. This modified design satisfied the inelastic Code criteria whereas the initial design failed to comply with the strain accumulation criterion.

INTRODUCTION

An ASME Class 1 structural component that does not comply with the elastic and simplified inelastic requirements of the elevated temperature Code Case N-47 requires a detailed inelastic analysis to show ASME Code compliance. It is difficult to judge, a priori, that a structural component which does not satisfy the elastic and simplified inelastic rules will satisfy inelastic requirements. One-dimensional simplified methods are of limited applicability, because the critical regions in the component are often located at a gross structural discontinuity where the thermal loading varies in the axial direction.

The purpose of this paper is to illustrate that although the elastic stress range is more than three times the yield strength of the material (316 stainless steel), it is possible to satisfy the ASME Code limits using a detailed inelastic analysis. Furthermore, it is not the stress range but the elastic stress intensities at various critical times during a thermal transient which provide better insight into the inelastic response of the structure.

This paper examines the Clinch River Breeder Reactor Plant (CRBRP) flued head containment penetration design. The purpose of the flued head, shown in Fig. 1, is to provide an attachment for the seal around the piping as it extends through the containment wall. Although the ratchetting strains are design limiting in the flued head design, the basic concepts presented in this paper on limiting the stress intensity during steady state operation are equally applicable to reduce creep-fatigue damage in structural components operating at elevated temperature [1][*]. The purpose here is to discuss concepts and not details of inelastic stress

[*]Numerals in brackets designate references at the end of this paper.

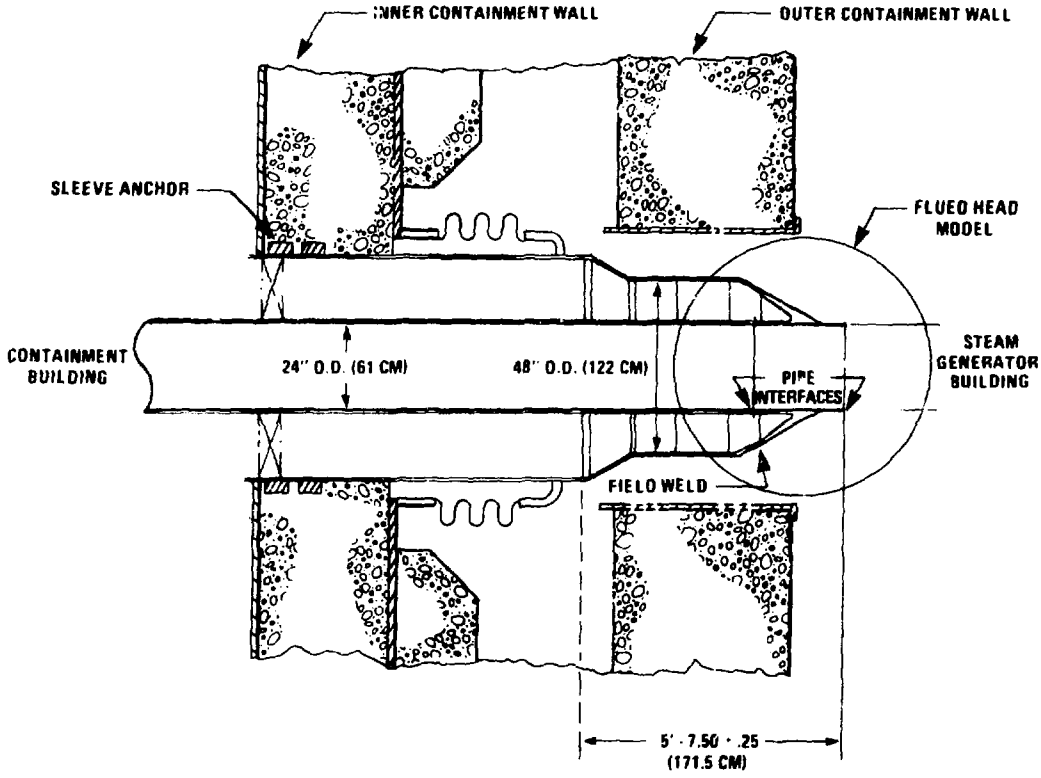

Figure 1. Longitudinal Cross Section of the CRBRP Intermediate Hot Leg Flued Head

analysis. In-depth discussion on computational methods in nonlinear analysis, validation of analysis methods, and modeling deformation behavior is provided in Chapter D--Elevated Temperature Design of the ASME sponsored book "Decade of Progress in Design Analysis" [2].

The initial inelastic analysis of the flued head model, that is circled in Fig. 1, resulted in excessive strain accumulation due to cyclic thermal loading. This is caused by the restriction of the free diametral movement of the thin-walled pipe by the conical support anchored in the containment wall. Based upon initial analysis results, two approaches are considered to reduce the restraint provided by the conical support. In the first approach, the rigidity of the cone is reduced by changing various geometric parameters of the flued head structure. However, within the design constraints, the overall stress range cannot be reduced significantly. In the second approach, heat flow path between the pipe and the cone support is altered by removing some insulation in the Y-section. That is, heat from the pipe is allowed to radiate from the hotter pipe to the colder cone regions. Although this modified insulation pattern slightly increases stress ranges during downshock thermal transients, the modification substantially reduces the elevated temperature steady state stress intensity. Since the structure experiences long time exposure at elevated steady state full power operation, this also improves the structural reliability of the component.

Previous analysis done by the Fast Flux Test Facility (FFTF) on flued heads is reported in [3]. The FFTF results show that all but one of the flued heads satisfy the ASME Code limits using elastic analysis. The remaining flued head requires inelastic analysis due to the combined effects of creep and fatigue; the operating temperature for this FFTF flued head is 1200°F (649°C). In contrast, the operating temperature of the CRBRP hot leg flued head is only 965°F (518°C) but the primary loads are significantly higher than in FFTF. This requires a considerbly thicker Y-section than is present in the FFTF flued heads. As a result, the CRBRP conical support is more rigid, which leads to a strain ratchetting problem.

DESIGN REQUIREMENTS AND ASSUMPTIONS

Thermal Loading

The CRBRP hot leg flued head experiences normal heat-up and cool-down events and upset and emergency events followed by a normal heat-up to the full power inlet fluid temperature of 965°F (518°C). These specified thermal transients vary in intensity and frequency of occurrence. An examination of the temperature changes occurring during these transient events shows that the specified 863 transient events can be conservatively placed into three groups to reduce cost of inelastic analysis. All severe downshock transients (a total of 59) are lumped into a 2U, uncontrolled rod withdrawal transient; other less severe but more frequently occurring upset

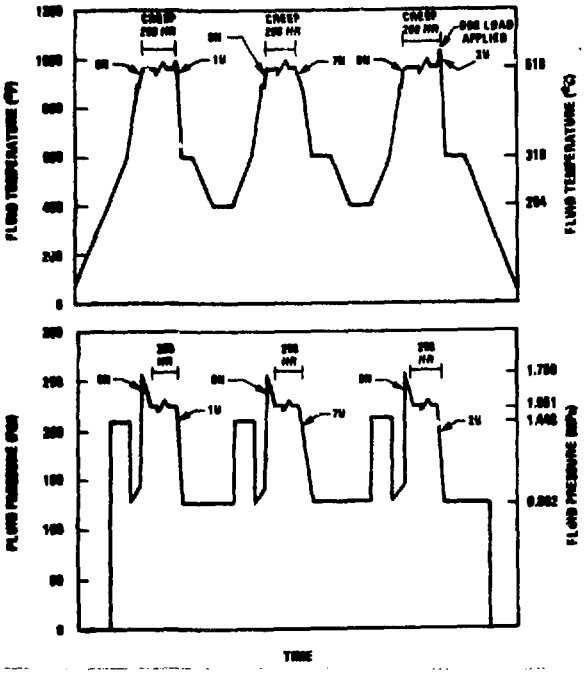

Figure 2. Typical Load Histogram for the Flued Head

transients (a total of 513) are lumped into 10, trip from full power transiant; and the final group contains 291 normal transients. The actual load histogram utilized in the inelastic analysis of the Flued Head is sketched in Fig. 2. To evaluate creep response, the transients are assumed to occur at constant intervals with 258 hours of full power creep hold time between transients. In addition, the equipment specification requires that the Operating

Basis Earthquake loading be included during these thermal transient events. These loads, as shown in Fig. 2, are conservatively included in the most severe transient.

Mechanical Loading

The mechanical loads are the pressure and the pipe loads. The pressure loading during full power is 225 psi (1.55 MPa), which reduces by about 50 percent during a downshock transient, as shown in Fig. 2. There are four types of pipe loads: axial and shear forces, and bending and twisting moments. The pipe loads act at the two interfaces of the containment penetration, as shown in Fig. 3. Each pipe load includes deadweight and thermal expansion loading. To reduce computational costs only an axisymmetric geometric model is considered for elastic as well as detailed inelastic analysis. Therefore, it is necessary to handle the nonaxisymmetric pipe loads in a conservative manner. This is accomplished by converting the bending and twisting moments into an equivalent moment and by utilizing the maximum bending stress (Mc/I) as a uniform axial stress applied to the pipe interface. This is combined with interface stresses due to uniform axial and shear loads. Since these idealized axisymmetric interface axial loads can act in either direction during a seismic event, four combinations of load directions are evaluated. The highest stress results from both interface axial loads acting in the direction of the containment (see Fig. 3). To ensure conservatism of this axisymmetric idealization, one elastic analysis has been performed on the axisymmetric geometry shown in Fig. 3 with actual nonaxisymmetric loading idealized as a Fourier series. The results show that the method of utilizing the maximum bending stress as a uniform axial stress produces the same maximum stress in the flued head as the actual bending moment distribution. Furthermore, the loads on the structure are thermal as well as mechanical. In fact, the predominant loads are due to thermal transients which actually produce axisymmetric stresses. Therefore, the axisymmetric loading assumption for the flued head is adequate.

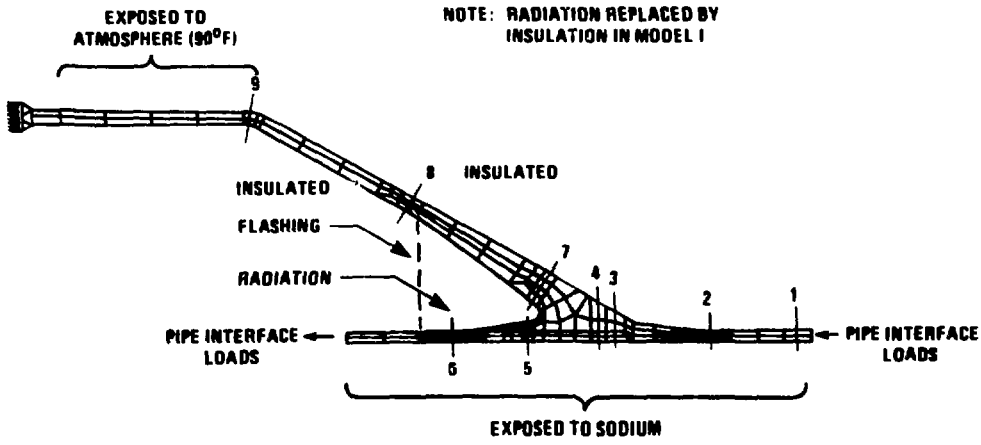

Figure 3. Axisymmetric Finite Element Model and Boundary Conditions (Model II)

Inelastic Analysis

The time-independent elastic-plastic and time-dependent creep analyses are performed according to the procedure outlined in [4]. These inelastic analysis recommendations are incorporated in the ANSYS [5] general purpose finite element computer program. This program has been extensively used to analyze structural components operating at elevated temperature and in the process has been verified and qualified satisfactorily for this application. The flued head is fabricated from 316 stainless steel (SS) material. Since the Flued Head is loaded from room temperature to 965°F (518°C) operating temperature, dependence of 316 SS material property variation is included in the analysis. Table 1 presents the avarage material properties at the operating temperature. The standard double exponential 316 SS creep equation is used for creep analysis.

TABLE 1. MECHANICAL PROPERTIES AT 965°F (518°C)

σ_y	=	18.69 Ksi (128 MPa)
E	=	23600 Ksi (162 GPa)
ν	=	.304
α	=	1.13×10^{-5} in/in/°F (2.03×10^{-5} cm/cm/°F)
E_p	=	1430 Ksi (9.86 GPa)

ELASTIC STRESS RANGE

Figure 3 shows the axisymmetric geometric idealizations of the flued head structure with nine critical sections for stress evaluation. The pipe diameter is 24 in. (610 mm), while the outer wall of the flued head has a 48 in. (1219 mm) diameter. A cone angled at 30° connects the two. Wall thickness of the pipe is 1/2 in. (12.7 mm) while the cone wall at Y-Section is 3/4 in. (19.1 mm) thick. All loads have been resolved into axial pressures so that the axisymmetric nature of the problem is maintained. Thermal boundary conditions consider convection between the inside pipe surface and the liquid sodium and convection between the outside surface of the cone and the ambient temperature of 90°F (32°C). The other surfaces are fully insulated.

In subsequent discussions, the terms stress intensity and stress range are used in context with the definitions provided in the ASME Code [6]. The stress intensity is the difference between the algebraically largest and the smallest principal stresses at a given point in the structure (simply twice the maximum shear stress). The definition of stress range is more complicated. Briefly, the principal stress differences, $S_{ij}=(S_i-S_j)$, are first calculated at a given point in the structure, with respect to specific points in time for a complete load cycle. The extremes through which each S_{ij} fluctuates during a load cycle defines the range of stress, S^r_{ij}. The maximum stress range, S^r_{max}, is the largest of the three S^r_{ij}'s.

Section 6 on the outside surface (see Fig. 3) experiences the highest primary stress intensity of about 13 ksi (90 MPa) due to primary thermal expansion and other mechanical loads. This region, near the geometric discontinuity, satisfies the primary load-controlled limits of the ASME Code [6]. In contrast, Section 5 experiences the largest secondary stress range due to downshock thermal transients. For example, the secondary stress ranges on the inside surface of Section 5 are 71 and 86 ksi (490 and 590 MPa) during 1U and 2U thermal transients, respectively. The stress ranges are higher during thermal transients because of different relative thermal expansions of the pipe and the cone. The mean temperature differential between the pipe and the cone is substantial during transients. Thus, the cone does not allow free thermal expansion of the pipe during thermal transient, which results in axial bending of the pipe. A small distance away from the junction of Section 5, this axial thermal bending produces hoop and axial stresses that are of opposite sign. At this relatively thin section, hoop and axial stresses due to the through-the-wall radial temperature differential, although of the same sign, are small. Hence, the radial temperature differential does not alter the predominant stress distribution caused by the axial thermal bending near the crotch region.

To satisfy the deformation limits of the ASME [6], the structure is evaluated according to Code Case N-47 [7] rules. Since the secondary stress range is greater than $3\sigma_y$, where σ_y is the yield stress of the material, it is not possible to satisfy the simplified inelastic rules of Code Case N-47. Even the simplified Bree method [8] predicts a total strain accumulation of 98% at the inside surface of Section 5.

In summary, the flued head design satisfied the primary load-controlled stress limits of the ASME Code; however, the elevated temperature strain and deformation limits are not satisfied using simplified inelastic analysis. In particular, the linearized bending strain accumulation predicted by the Bree method is about 50 times the allowable strain accumulation. As is shown below, the Bree method is unrealistic in this case where axial temperature differential causes axial bending in axisymmetric structures. It is necessary to perform a detailed inelastic analysis to compute realistic strain accumulation in the structure.

INELASTIC ANALYSIS I (INITIAL DESIGN--CASE 1)

The flued head is subjected to five load cycles consisting of thermal transients similar to those sketched in Fig. 2. OBE events are applied only in the first two cycles. (Results for the five remaining OBE events are conservatively estimated from these first two cycles.) The analysis is performed according to the guidance provided in [4], with the ANSYS computer program [5]. During the first heat-up, even before any downshock thermal transients are applied, plastic strains are incurred at the critical Section 5 near crotch region. The plastic zones before and after the first downshock (1U thermal transient) are shown in Fig. 4a and 4b, respectively. After the first down transient (Fig. 4b), the cone section also yields; and after three load cycles, as shown in Fig. 4c, the plastic zone spreads along the inside surface of the pipe below the crotch and along the outside surface of the pipe. No further increase in the size of the yield zone occurs beyond three cycles of loading.

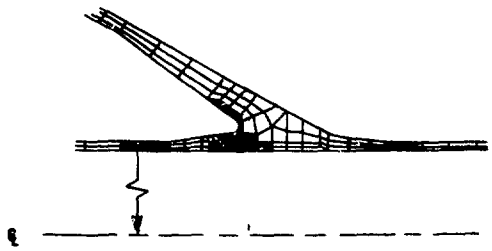

Figure 4a. Model I - Plastic Zone Size After First Heat Up

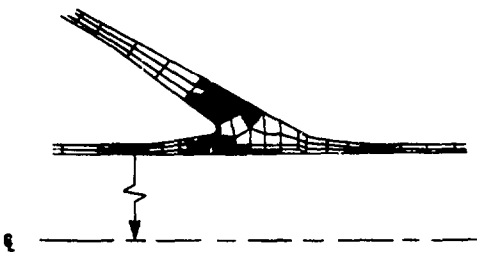

Figure 4b. Model I - Plastic Zone Size After First Thermal Downshock

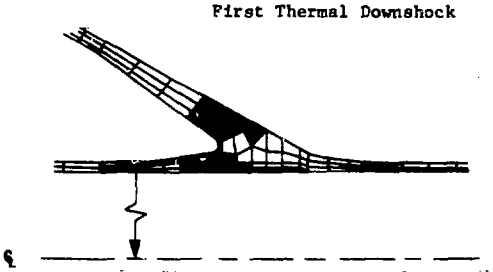

Figure 4c. Model I - Plastic Zone Size After Three Load Cycles

The deformed geometry plots in Figs. 5a and 5b show movement of the structure before and after the first downshock thermal transient. Free radial thermal expansion in both cases is about 0.5 in. (12.7 mm). At the critical Section 5 a convex inward bulge at the inside surface can be seen in Fig. 5a at the maximum temperature of 1050°F (566°C); whereas in Fig. 5b at a temperature of 600°F (316°C) the cone restrains the pipe from free contraction which induces a concave profile at this section. Thus, the cone acts as a partially rigid support which prevents free thermal expansion of the pipe during thermal transients. This flexes the pipe in the axial direction, and cyclic axial bending is the primary source of plastic ratchetting in the pipe. Figure 6 shows plastic ratchetting strains accumulated per cycle at the inside and outside surfaces of the pipe and the membrane values at Section 5. Interestingly, the inside surface yields first and experiences the highest equivalent stress, but the ratchetting strains are higher on the outside surface. The strain on the outside surface accumulated for the design life of the structure exceeds the strain limit specified in Code Case N-47.

The spread of plastic zones in Fig. 4c shows a skewed distribution of plastic zone in the straight pipe. Although the initial plastic strains on the inside surface are high at Section 5, the plastic ratchetting strains are higher on the outside surface because the axial bending is not symmetric about the middle surface. However, this observed plastic ratchetting behavior is difficult to anticipate from the elastic linearized stress intensities presented in Table 2. As discussed earlier, it is the rigidity of the conical support which restrains free thermal expansion of the pipe, thus flexing pipe Section 5 during heat-up and cool-down. The rigidity of the pipe can be reduced either geometrically, by designing it as thin as possible, or by equalizing the temperature distribution between pipe Section 5 and cone Section 7.

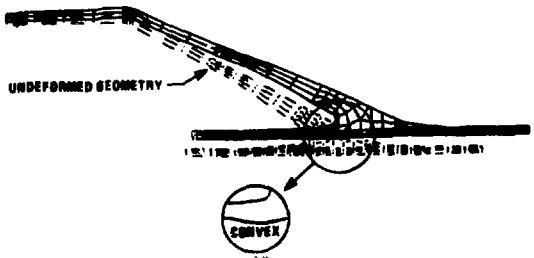

Figure 5a. Deformed Geometry at Fluid Temperature of 1050°F (566°C)

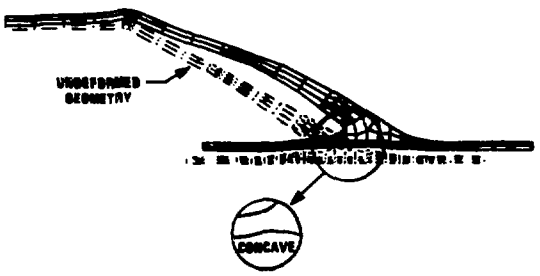

Figure 5b. Deformed Geometry at Fluid Temperature of 600°F (316°C), Approximately 800 Seconds After 2U Downshock

GEOMETRIC OPTIMIZATION OF SUPPORT CONE

Since the high stresses in the Y-section are induced by the rigidity of the cone with respect to the pipe, one is led to consider a corresponding decrease in the stiffness of this region. Two geometric modifications are evaluated to reduce the stiffness of the cone support: a) thinning the cone at the Y intersection, b) changing the angle of the cone pipe intersection. The first supplemental model (SM-I) changes the thickness of the cone from three-quarters to one-half inch, thus making it more flexible. The second supplemental model (SM-II) also employs the decreased cone thickness but uses a reduced intersection angle (20° instead of 30°) between the cone and the pipe. The reasoning behind the change of angle is that the stiffness is a maximum for thermal radial gradients when the intersection angle is 90° and a minimum at 0°. Both SM-I and SM-II showed a decrease in the

primary-plus-secondary stress range (22% and 14%, respectively) at Section 5. However, the most highly stressed region now occurs on the cone at Section 7. The maximum primary-plus-secondary stress range shows no decrease (SM-II) or slight increase (6% for SM-I). In addition, both have much larger inelastic strain predictions by the Bree method [8] than the original model.

In summary, attempts to reduce the pipe support cone restraint by modifying the cone geometry were not successful. Therefore, the option of equalizing the temperature distribution in the Y intersection region, especially during steady state operation, is investigated.

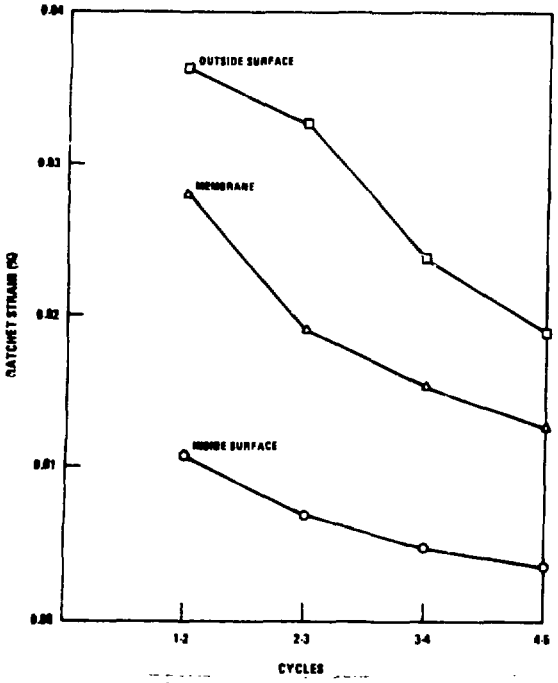

Figure 6. Model I - Plastic Ratchet Strain Per Cycle at Section 5

TABLE 2. STRESS INTENSITY - INITIAL DESIGN Case 1.

Thermal Loading	Linearized Stress Intensity Inside (psi)	Outside (psi)
Steady State	+27162	-18437
U1 - 70 Secs	+30871	-19179
U1 - 700 Secs	-36964	-22460
U2 - 400 Secs	+42867	-27750
U2 - 1200 Secs	-39744	+23301

Notes: 1 Ksi = 6.894757 MPa.
Maximum stress range for U1 transient = 67835 psi
Maximum stress range for U2 transient = 82611 psi

TEMPERATURE DISTRIBUTION IN Y-SECTION

The space between the pipe and the cone in the Y-section (Fig. 3) is fully insulated; hence, the heat flow between the pipe Section 5 and the cone Section 7 is through the thick metal ring Section 4. The temperature differential between these two sections is large, especially during steady state operation. One way to equalize the temperature distribution is to provide a direct path for heat flow between the cone and the pipe. This can be done by removing a block of insulation, shown in Fig. 3, to permit heat transfer by radiation between the pipe and the cone.

Figure 7 shows the mean temperature in the pipe (Section 5) and the cone (Section 7) during U2 transient for two cases:

1) Case 1 with insulation
2) Case 2 without insulation.

Table 3 presents the linearized elastic stress intensity for Case 2. The ratio of the stress intensities of Case 2 to Case 1 (presented in Table 2) during steady state operation is about one half. Interestingly, the difference in mean temperature between the pipe and the cone also maintains the one-half ratio when comparing Case 2 to Case 1, as can be seen in Fig. 7. Conversely, Fig. 7 also shows that during downshock thermal transient the temperature difference between the pipe and cone is higher for Case 2 than for Case 1. Consequently, the stress intensities for U1 and U2 downshock transients are slightly higher for Case 2 than for Case 1. Thus, by investigating only the elastic stress ranges during U1 and U2 events one could come to the conclusion that the Case 1 insulation design is better because the stress ranges are lower than those for Case 2. But this conclusion could be misleading, because it is not just the stress range during a transient event that is important, but also the stress intensity during steady state elevated temperature operation. The stress intensity for Case 1 during steady state is nearly double that for Case 2. It is desirable to lower the stress intensity during steady state elevated temperature operation even if the stress range is slightly increased during downshock transients, because in actual operation a structural component experiences long periods of creep hold time at steady state stresses. Furthermore, during steady state operation, the stress intensity (Tresca stress) for Case 2 is less than the yield stress of the material at operating temperature, whereas the stress intensity for Case 1 is 1.5 times the yield stress. These considerations are important in pursuing inelastic analysis of the structure without insulation (Case 2).

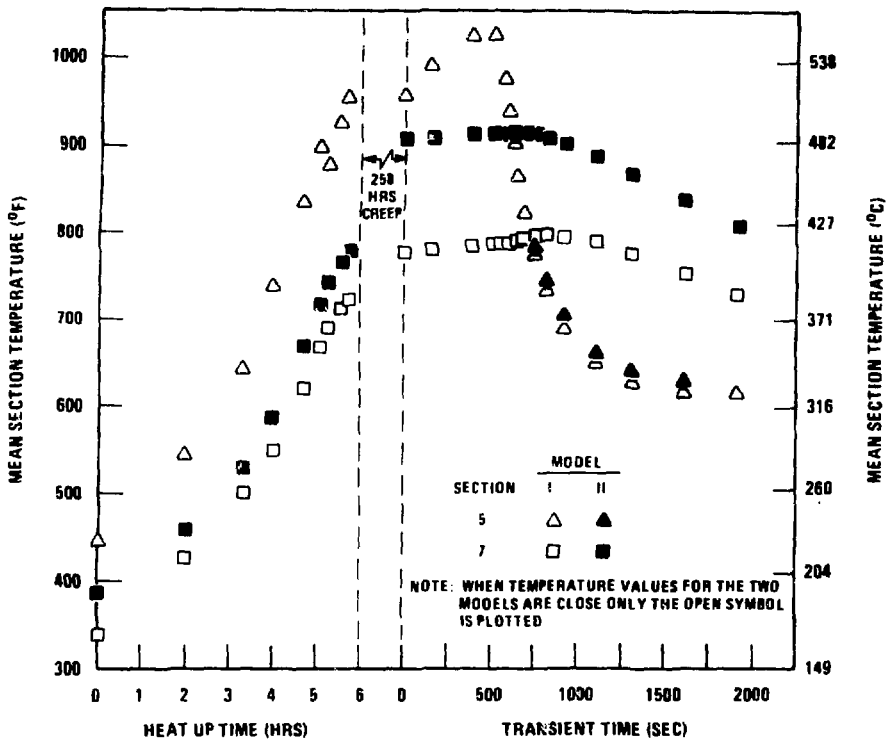

Figure 7. Mean Section Temperature During the 2U Transient

TABLE 3. STRESS INTENSITY - REFINED DESIGN Case 2.

Thermal Loading	Linearized Stress Intensity Inside (psi)	Outside (psi)
Steady State	+11740	-7870
U1 - 70 Secs	+15880	-8220
U1 - 900 Secs	-56420	+32680
U2 - 390 Secs	+28760	-16520
U2 - 1000 Secs	-60130	+32210

Notes: 1 ksi = 6.894757 MPa.
Maximum stress range for U1 transient = 72300 psi
Maximum stress range for U2 transient = 88890 psi

INELASTIC ANALYSIS II (REFINED DESIGN--CASE 2)

The finite element model for thermal and inelastic stress analysis is identical to the earlier model shown in Fig. 3. For completeness, a discussion of the radiation shape factors for the thermal analysis of the conical section are presented in Appendix I. The thermal, as well as stress, analyses are performed using the ANSYS computer program [5]. A total of 12 load cycles were analyzed to comply with Code Case N-47 strain accumulation requirements. The loading sequence is similar to that sketched in Fig. 2. Of the 12 cycles, the 2U event is included in only five, the first two and the last two. In the other seven cycles, another 1U replaces the 2U. This keeps the severity of thermal events in close proportion to the number of severe transients postulated in design specifications. The 2U occurs less frequently but is more severe than the 1U transient. This is reflected in the selection of the thermal load histogram, where the number of 2U (and 1U) events that are necessary to satisfy the ASME Code Criteria are included in the analysis.

The structural response is plastic during initial heat-up; but as the structure reaches its steady state temperature distribution, the stresses reduce into the elastic regime. During downshock, thermal transient plastic strains are incurred near the Y-section; the spread of plastic zones at the end of 3 load cycles is shown in Fig. 8. Plastic zones remained unchanged for the rest of the load cycles. The distribution of plastic zones predicted by this second analysis, where the heat is allowed to radiate from the pipe to the cone support, is different from the first analysis discussed earlier. For example, in Fig. 8 the distribution of plastic zone in the pipe is uniform across the thickness around Section 5 when compared with the distribution observed earlier in Fig. 5c. This difference provides a more uniform response, in terms of plastic ratchetting strains, to the axial bending of the pipe due to the thermal restraint offered by the support cone.

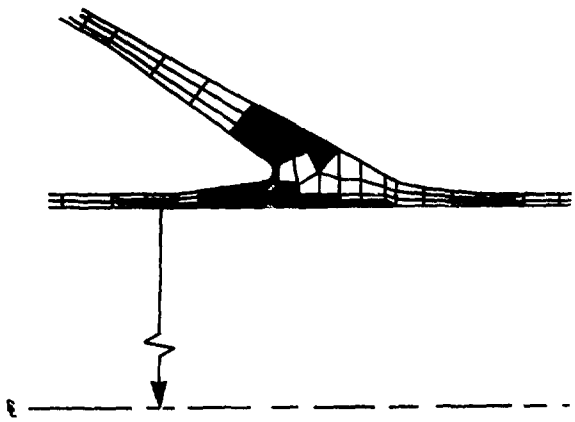

Figure 8. Model II - Plastic Zone Size After Three Load Cycles

Figure 9 shows the deformation of the inside surface during 965°F (518°C) elevated temperature steady state operation and during the most severe mean temperature differential between the pipe and the cone, for the 1U transient at about 600°F (316°C) pipe temperature. These deformations are shown for both analyses: Case 1 with insulation and Case 2 with radiation heat flow from the pipe to the cone support. As noted earlier, the steady state stress intensity for Case 1 is about half of that for Case 2; the maximum radial displacements during steady state also reflect this difference: δ_{2s} is about $0.56\delta_{1s}$. On the other hand, the stress ranges during downshock transients for Case 2 are about 10% higher than for Case 1; the maximum radial displacements reflect this difference: δ_{2t} is about 1.46_{1t}. The maximum stress intensity during the 1U transient for Case 2 is about 1.5 times that for Case 1. Of course, there is no one-to-one correspondence between elastic stress ranges and inelastic displacements. Stress ranges are simple functions of temperature only to the point that the elastic material properties are functions of temperature. There is no way to factor in the inelastic response at temperature. The important point is that the inelastic deformations are reduced if the maximum stresses occur at lower than operating temperature; because at a lower temperature the yield strength of the material is higher than at operating temperature. Hence, it is desirable to have the maximum stress intensity occur at lower temperatures as in Case 2. Also, the deformation of the inside surface, shown in Fig. 9, clearly indicates that the Case 2 deformation pattern during elevated temperature operation is preferable, because the total deformations along the length of the pipe are less than those predicted for Case 1. On the other hand, at the end of downshock transient (316°C) the maximum deformation predicted for Case 2 is substantially higher than that for Case 1. This too is preferable from the structural integrity point of view, because the postulated severity and frequency of thermal transients may or may not occur during actual plant operation; whereas the postulated steady state elevated temperature periods will most probably be experienced during 100% power plant operation.

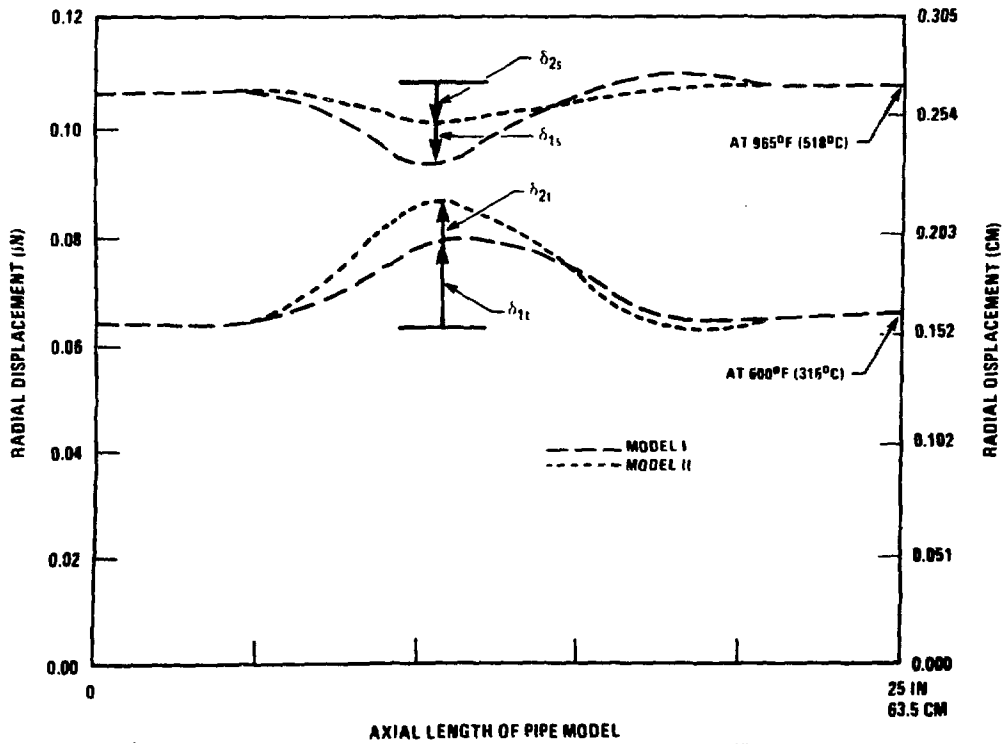

Figure 9. Radial Displacement of the Inside Pipe Surface

Ratchet Strains

Case 1 analysis predicted the highest ratchet strains occurred near Section 5 in the pipe, as shown in Fig. 6. Figure 10 shows the strain increment per cycle predicted by Case 2 analysis at Section 5. It is at the outside surface that the strain accumulation exceeded Code Case N-47 allowable limits in the initial Case 1 analysis. Therefore, in the refined Case 2 analysis points on the outside surface around Section 5 are searched to find the maximum strain accumulation. Figure 11 shows strain increments per cycle on the outside surface at Section 5a to 5d; of these Section 5c experiences the largest strain accumulation. From these results strain accumulation at the outside surface for the design life is projected to satisfy the 2% linearized surface strain limit specified in the Code.

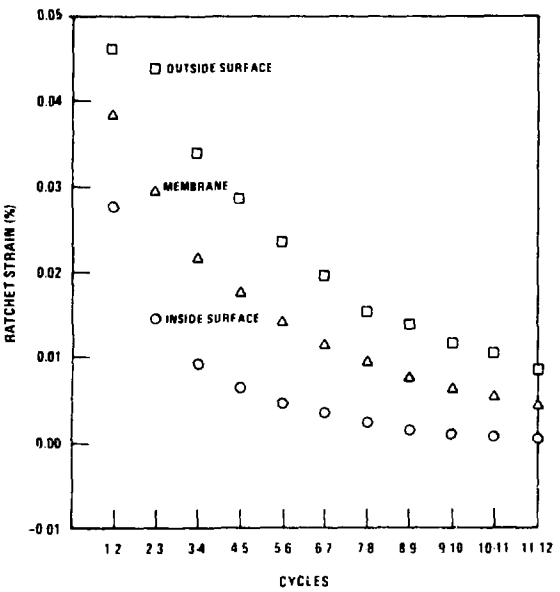

Figure 10. Model II - Plastic Ratchet Strain Per Cycle at Section 5

A direct comparison between the initial and refined models can be made by examining the membrane values in Figure 6 (Model I) and the values for Section 5a in Figure 11 (Model II). Between the first and second cycles, Model II has a greater membrane strain increase than Model I (.0354% to .0282%). However, between the fourth and fifth cycles, the ratchet strain increase is greater for Model I (.0126% to .0124%). Since the rate of decrease is greater in Model II, strain accumulation extrapolated to end of plant life satisfies the Code criteria.

Incidentally, a simplified CHERN thick cylinder inelastic analysis [9] of the structure has been performed to compute ratchetting strains. The simplified analysis substantially underpredicts the ratchetting strains. This confirms earlier observation [1] that simplified axisymmetric inelastic prediction methods are unconservative for structures with axial temperature differential or an axial constraint which induces axial bending in axisymmetric structures.

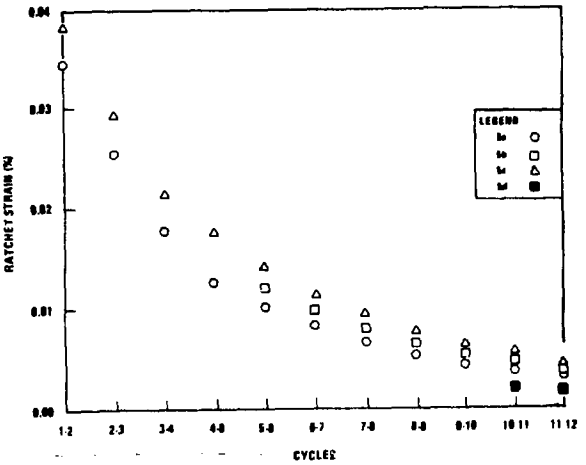

Figure 11. Membrane Ratchet Strain at Various Cross Sections Near Section 5

CONCLUDING REMARKS

The inelastic analysis results presented in this paper illustrate that the elastic stress range is not a satisfactory indicator of the inelastic behavior of this structure. For example, a slight increase in stress range improved the overall response of the flued head structure, which could not be determined a priori from elastic results. More importantly, it is the stress intensity, at various critical times during a thermal transient event, that provides more insight into the inelastic structural response. The temperature differential between various parts of the structure can be changed without significantly altering the overall elastic stress range experienced by the structure. Consequently, with some modification in the insulation pattern, it is possible to arrive at a balanced heat flow, especially during elevated temperature steady state full power operation. In an earlier design of the FFTF/IHX shear key forging ring [1], change in insulation patterns and modification of heat flow paths were necessary not only to minimize ratchetting strain but also to reduce the creep-rupture damage accumulation in the structure.

A specific example of the flued head design, discussed in this paper, illustrates that a reduced axial temperature differential improved the overall structural design by reducing cyclic axial bending in the critical region. This reduced cyclic axial bending, as well as lower stress intensity during steady state normal operating condition reduced strain accumulation due to ratchetting at the most highly stressed location in the flued head. Fortunately, the reduced stress during steady state creep hold time also reduces creep-rupture damage without significantly altering th fatigue damage at the same location.

ACKNOWLEDGEMENTS

This paper is based upon work performed for the U.S. Department of Energy under Contract E4-76-C-15-2395 as a part of the CRBRP Project. The authors express their appreciation to Dr. R. H. Mallett and Mr. R. M. Mello for their valuable suggestions and comments during the course of this investigation.

REFERENCES

[1] A. K. Dhalla and R. V. Roche, "Inelastic Analysis and Satisfaction of Design Criteria of a High Temperature Component", in Advances in Design for Elevated Temperature Environment, Eds. S. Y. Zamrik and R. I. Jetter, pp. 83-92, American Society of Mechanical Engineers, N.Y., 1975.

[2] Decade of Progress, American Society of Mechanical Engineers, N.Y. 1981 (to be published).

[3] R. C. Sampson, "Stress Analysis of Conical Flued Heads for FFTF Liquid Metal Piping Anchors," in Elevated Temperature Piping Design, Eds. L. V. Severud and A. H-C. Marr, American Society of Mechanical Engineering, 1979.

[4] C. E. Pugh and D. N. Robinson, "Some Trends in Constitutive Equation Model Development for High-Temperature Behavior of Fast-Reactor Structural Alloys," Nucl. Eng. Des. 48, pp. 269-276 (1978).

[5] J. Gabriel, J. DeSalvo, and J. A. Swanson, ANSYS Engineering Analysis System, User's Manual, Swanson Analysis Systems Inc., Elizabeth, PA 1975.

[6] ASME Boiler and Pressure Vessel Code "Section III, Nuclear Power Plant Components," American Society of Mechanical Engineers, New York, 1977.

[7] ASME Boiler and Pressure Vessel Code Cases, Case N-47 (1592), "Class 1 Components in Elevated Temperature Service, Section III, Division 1," American Society of Mechanical Engineers, New York, 1977.

[8] J. Bree, "Elastic-Plastic Behaviour of Thin Tubes Subjected to Internal Pressure and Intermittent High-Heat Fluxes with Application to Fast-Nuclear-Reactor Fuel Elements", J. Strain Anal. 2, pp. 226-238 (1967).

[9] J. M. Chern and D. H. Pai, "Inelastic Analysis of a Straight Tube Under Combined Bending Pressure and Thermal Loads", Trans. ASME, J. of Press. Vessel Tech., 97, pp. 155-162 (1975).

APPENDIX I

SHAPE FACTORS

The section of the Flued Head involved in the radiation heat transfer has a complicated geometry. A few simplifying assumptions are necessary to solve the problem. Elements comprising the surface are assumed small enough such that no axial variation is considered. The shape factor for two given elements is a function of the angular variation only. The second assumption idealizes the geometry such that the pipe is considered to be of constant thickness (even near the cone intersection) and that the curvature in the Y-section is replaced by a small plate parallel to the flashing and perpendicular to the pipe. Any shape factor represents the amount of radiation from a point to a finite area. Only a point need be considered; because no axial variation is considered, and the radiating element is axisymmetric. The general formula for the shape factor is

$$\frac{1}{\pi}\int \frac{\cos\beta_1 \cos\beta_2}{s^2} \, dA_2$$

where:

A_2 = area of element receiving radiation

dA_2 = elemental area receiving radiation, $rtd\theta$

r = distance of dA_2 from centerline

t = axial length of elemental area

θ = angular variation about the centerline

s = distance from radiating point to dA_2 (function of θ only)

β_1 = angle between s and normal of radiating surface at radiating point

β_2 = angle between s and normal of dA_2

Five basic types of integration problems are investigated: 1) radiation from pipe to the cone, 2) radiation from the pipe to the flashing (or plate in the Y-section - it is the same type of problem), 3) from one section of the cone to another section at a different axial location, 4) from the cone to the flashing (or parallel plate in the Y-section), and 5) from the flashing to the parallel plate to the Y-section. Although the algebra and integration are tedious, they are straightforward. The difficult task is to calculate the limits of the angular integration. In all five cases the radiating surface point does not see the entire surface receiving radiation, because the pipe obstructs the radiating at path. Therefore, the integration limit, A_2, is only that part of the surface seen by the radiating point.